Supporting Information for "Fault-zone damage promotes pulse-like rupture and back-propagating fronts via quasi-static effects"

B. Idini*[1] and J.-P. Ampuero[2]

[1]Seismological Laboratory, California Institute of Technology, 1200 E. California Blvd., Pasadena, CA 91775, USA

[2]Université Côte d'Azur, IRD, CNRS, Observatoire de la Côte d'Azur, Géoazur, 250 Rue Albert Einstein, 06560 Valbonne, France

Contents of this file

1. Text S1 to S4
2. Figures S1 to S6
3. Tables S1 to S2

Introduction Text S1 describes the methodology used in Section 3. Text S2 and S3 are mathematical derivations of results presented and discussed in the main text. Figures S1-S2 and S4 show supplementary aspects of the methodology used in Section 3. Figures S3 and S5 show supplementary results to those presented in the main text. Figure S6 is a summary of LVFZ properties contained in the literature. Table S1 describe supplementary

Corresponding author: B. Idini, Seismological Laboratory, California Institute of Technology, 1200 E. California Blvd., Pasadena, CA 91125, USA. (bidiniza@caltech.edu)

information relative to our results in Section 3. Table S2 contains information required to reproduce our results in Section 3.

Text S1: Earthquake cycle simulations

Methods. We characterize the effect of a LVFZ on rise-time and slip profile in earthquake cycle simulations covering a wide range of values of LVFZ thickness and damage. We adopt a spectral boundary integral equation method (SBIEM) (Luo et al., 2017) and a quasi-dynamic approximation where wave-related effects are crudely represented by a radiation-damping term (Rice, 1993). The static stress transfer kernel required in the SBIEM for a LVFZ is derived in Text S2. The modeling approach captures the static LVFZ effects described in Section 2 of the main text, without including any dynamic effect of fault zone reflected waves, and its computational efficiency enables a comprehensive exploration of the parameter space.

The fault strength is prescribed by the Dieterich-Ruina rate-and-state friction law coupled with the "ageing law" of state evolution (Dieterich, 1981; Ruina, 1980, 1983):

$$\tau/\sigma = \mu_0 + a \ln\left(\frac{V}{V_0}\right) + b \ln\left(\frac{V_0\theta}{D_c}\right) \tag{1}$$

$$\dot{\theta} = 1 - \frac{V\theta}{D_c} \tag{2}$$

where τ and σ are the shear and normal fault stresses, respectively, V is slip rate and θ a fault state variable. The parameter a quantifies the direct effect, b the evolution effect, and D_c is the characteristic slip related to the state evolution. Under steady-state, $b > a$ leads to stick-slip behavior (velocity-weakening, VW) whereas $b < a$ leads to stable sliding behavior (velocity-strengthening, VS). We represent a seismogenic zone driven by

surrounding creep by prescribing a VW patch of length L_{vw} in the middle of the fault, surrounded by two VS segments of total length $3L_{vw}$ and, at further distance, by steady uniform creep at slip rate V_{pl} (Fig. S2). The parameter values of our numerical model are given in Table S2.

Ruptures that start as a crack and later turn into a pulse require a minimum rupture distance to develop the transition, therefore a sufficiently large ratio between L_{vw} and the nucleation length L_{nuc} (Rubin & Ampuero, 2005):

$$L_{nuc} = \frac{2}{\pi} \frac{\mu D_c b}{\sigma (b-a)^2} \tag{3}$$

Previous earthquake cycle simulations including a LVFZ model did not show significant reductions in rise-time for $L_{vw} \sim 1.5 L_{nuc}$ and $\Delta = 0.36$ (Kaneko et al., 2011), so we extended the seismogenic length to $L_{vw} \sim 10 L_{nuc}$. Moreover, we explored values of Δ ranging from moderate damage to the upper bound inferred from current seismological observations ($\Delta = 0.5 - 0.9$) and values of h extending over a range wide enough to encompass most geological and seismological observations ($2h/L_{vw} \sim 10^{-3} - 10$). A compilation of observed or estimated levels of damage and fault-zone thickness in natural faults is given in Fig. S6.

We prescribed a minimum of five elements within an effective cohesive zone,

$$L_b^* = \frac{9\pi}{32} \frac{\mu^* D_c}{\sigma b}, \tag{4}$$

where μ^* is an effective shear modulus that accounts for the LVFZ derived bellow. A well-resolved cohesive zone was verified a posteriori in all our simulation results, characterized by a smooth and properly sampled stress distribution near the rupture tips.

Estimation of the process zone size in a LVFZ. The components of slip and stress drop at a wavenumber k^* are related by an effective shear modulus, μ^*, which represents an effective value of the shear modulus profile $\mu(x)$ up to an off-fault distance comparable to $\lambda^* = 2\pi/k^*$. As is the case of a homogeneous medium, the static stress transfer at this effective length scale can be written as:

$$\mathcal{K}(k^*) = \frac{1}{2}\mu^*|k^*| \tag{5}$$

Combining equations (17) and (5), we obtain:

$$\mu^* = \mu(1-\Delta)\coth(h|k^*| + \operatorname{atanh}(1-\Delta)) \tag{6}$$

An estimate of the process zone size in a LVFZ, L_b^*, is related to the process zone size in an intact medium, L_b, by:

$$L_b^* = L_b\frac{\mu^*}{\mu} \tag{7}$$

After replacing Eq. (6) into Eq. (7) and setting $\lambda^* \approx L_b^*$, the process zone in a LVFZ satisfies:

$$L_b^* = L_b(1-\Delta)\coth\left(\frac{2\pi h}{L_b^*} + \operatorname{atanh}(1-\Delta)\right) \tag{8}$$

This equation is solved numerically to obtain L_b^*/L_b as a function of Δ and h/L_b.

Text S2: The static stress transfer kernel in a LVFZ model.

Problem statement. Let us consider a 2D elastic medium where the fault is located on the line $x = 0$. The medium is heterogeneous with the shear modulus μ depending only on x. Slip is anti-plane in the direction out of the $x - y$ plane. A static slip distribution $\mathcal{D}(y)$ produces a shear stress on the fault $\mathcal{T}(y)$. Because the elasticity problem is linear,

slip and stress are related by a linear relation:

$$\mathcal{T}(y) = -\int_{-\infty}^{\infty} \mathcal{K}(y, y')\mathcal{D}(y')dx', \tag{9}$$

where $\mathcal{K}$ is the static stress transfer kernel. The minus sign is introduced to give $\mathcal{K}$ a meaning analogous to stiffness in a spring-block system. As the problem is invariant by translation along y ($\mathcal{K}(y, y') = \mathcal{K}(y - y')$), Eq. (9) is a convolution:

$$\mathcal{T}(y) = -\int_{-\infty}^{\infty} \mathcal{K}(y - y')\mathcal{D}(y')dy' \tag{10}$$

After a Fourier transform, the convolution simplifies into a product:

$$\mathcal{T}(k) = -\mathcal{K}(k)\mathcal{D}(k), \tag{11}$$

where k is the wavenumber along the fault direction, y. In order to connect stress and slip in the fault, the goal is to derive an expression for the static kernel in spectral domain, the so-called spectral stiffness $\mathcal{K}(k)$.

The equation of anti-plane elasticity governing the displacement field $u(x, y)$ parallel to z is:

$$\mu(x)u_{,yy} + (\mu(x)u_{,x})_{,x} = 0 \tag{12}$$

A first boundary condition is the symmetric distribution of applied slip on each side of the fault:

$$u(0^{\pm}, y) = \pm\frac{1}{2}\mathcal{D}(y) \tag{13}$$

A second boundary condition requires that displacement u must be finite at $x = \pm\infty$. As the boundary conditions are symmetric, the resulting displacements are symmetric as well and follow $u(-x, y) = -u(x, y)$. Therefore, we solve for the half-plane $x \geq 0$ only.

After applying a Fourier transform over Eq. (12), our task is reduced to find $u(x,k)$ such that:

$$\begin{aligned} -k^2\mu(x)u + (\mu(x)u_{,x})_{,x} &= 0 \\ u(0^+,k) &= \frac{1}{2}\mathcal{D}(k) \\ u(\infty,k) &< 0 \end{aligned} \tag{14}$$

and then evaluate the fault shear stress $\mathcal{T}(k) = \mu(0)u(0,k)_{,x}$.

The problem has analytical solutions only for certain shear-modulus distributions $\mu(x)$. In the following we address two cases: a homogeneous medium and a two-layer medium. An analytical solution for an exponential distribution of $\mu(x)$ is possible as well but not exposed here (Ampuero et al., 2002).

Homogeneous medium. In a homogeneous medium, Eq. (12) reduces to:

$$-k^2u + u_{,xx} = 0, \tag{15}$$

Its well-known general solution is $u(x,k) = A\exp(-|k|x) + B\exp(|k|x)$. The finite displacement boundary condition imposes $B = 0$, and the fault boundary condition at $x = 0$ implies $A = \frac{1}{2}\mathcal{D}$. The resulting displacement is $u(x,k) = \frac{1}{2}\mathcal{D}(k)\exp(-|k|x)$. After evaluating the shear stress on the fault, $\mathcal{T}(k) = -\frac{1}{2}\mu|k|\mathcal{D}(k)$, the spectral stiffness is:

$$\mathcal{K}(k) = -\mathcal{T}(k)/\mathcal{D}(k) = \frac{1}{2}\mu|k| \tag{16}$$

Two-layer medium. Consider a fault in a homogeneous medium surrounded by two layers of uniform half-thickness h and homogeneous but reduced shear modulus (Fig. 1b). Within the layers the shear modulus is $\mu(1-\Delta)$ and outside the layers it is μ. The deriva-

tion of the kernel in a layered medium follows the same steps as the previously addressed case. The differential equation is Eq. (15). Its general solution is a combination of exponential functions for each layer, together with a total of four new constants analogous to A and B. Two new boundary conditions arise: continuity of displacement and stress across the interface between the layers, $u(h^+, k) = u(h^-, k)$ and $(1 - \Delta)u(h^-, k)_{,x} = u(h^+, k)_{,x}$.

It is possible to obtain the displacement $\mathcal{D}(x, k)$ after some algebraic work, then derive the shear stress at the fault and finally the spectral kernel:

$$\mathcal{K}(k) = \frac{1}{2}\mu|k|(1 - \Delta)\coth(h|k| + \operatorname{atanh}(1 - \Delta)) \tag{17}$$

Static slip profiles with constant stress drop. A first application of Eq. (17) is to numerically compute the static slip profiles of a rupture with prescribed constant stress drop propagating in a fault with a LVFZ (Fig. 1c). By applying an inverse fast Fourier transform to Eq. (17) over a very long fault, we obtained a static stress transfer kernel in space domain, $\mathcal{K}(y)$. Then assuming a uniform stress drop, we solved numerically the discretized version of Eq. (10) to obtain the slip profiles.

Numerical implementation of a LVFZ. Our numerical implementation of a LVFZ on multi-cycle earthquake simulations consists of combining the time-domain kernel of a fault with finite length (Cochard & Rice, 1997) with Eq. (17) in the frequency domain. The numerical models shown in Fig. 3 are based on this implementation. We verified that the values of the obtained kernel are similar to those obtained by the more expensive approach of applying Eq. (17) to a periodic homogeneous fault 32 times longer (Fig. S4).

Text S3: The stress transfer in a LVFZ and a Burridge-Knopoff model.

Burridge-Knopoff (BK) model. In a BK model (Burridge & Knopoff, 1967), the quasi-static slip $\mathcal{D}_i$ and stress $\mathcal{T}_i$ at the base of the i-th block of area dy^2 relate to each other as:

$$\mathcal{T}_i dy^2 = -k_L(\mathcal{D}_i - \mathcal{D}_L) + \bar{\mathcal{K}}(\mathcal{D}_{i-1} - 2\mathcal{D}_i + \mathcal{D}_{i+1}), \tag{18}$$

where $\mathcal{D}_L$ is the loading displacement, k_L the loading stiffness, and $\bar{\mathcal{K}}$ the stress transfer due to the relative motion of the sliders. We furthermore introduce a loading stiffness per unit area of block surface defined as:

$$\bar{\mathcal{K}}_L = k_L/dy^2 \tag{19}$$

Taking the continuum limit ($dy \to 0$) in Eq. (18):

$$\mathcal{T}(y) = -\bar{\mathcal{K}}_L(\mathcal{D}(y) - \mathcal{D}_L) + \bar{\mathcal{K}}\mathcal{D}_{,yy} \tag{20}$$

The second term in the right-hand side in the equation above is derived by expanding terms in a Taylor series up to second order at small dy:

$$\mathcal{D}_{,yy} \approx \frac{\mathcal{D}(y-dy) - 2\mathcal{D}(y) + \mathcal{D}(y+dy)}{dy^2} = \frac{\mathcal{D}_{i-1} - 2D_i + \mathcal{D}_{i+1}}{dy^2} \tag{21}$$

Taking the Fourier transform for non-zero wavenumbers ($|k| > 0$):

$$\mathcal{T}(k) = -\bar{\mathcal{K}}_L\mathcal{D}(k) - \bar{\mathcal{K}}k^2\mathcal{D}(k) = -(\bar{\mathcal{K}}_L + \bar{\mathcal{K}}k^2)\mathcal{D}(k) \tag{22}$$

The loading displacement $\mathcal{D}_L$ is spatially uniform, hence it only contributes when $k = 0$. We get the following static kernel in spectral domain:

$$\mathcal{K}(k) = \bar{\mathcal{K}}_L + \bar{\mathcal{K}}k^2 \tag{23}$$

Static slip induced by uniform stress drop in the continuum BK model. Consider a uniform stress drop within a rupture segment of size r, i.e.

$$\Delta\tau = \bar{\mathcal{K}}_L \mathcal{D}(y) - \bar{\mathcal{K}} \mathcal{D}_{,yy} \tag{24}$$

for $y \in [-r/2, r/2]$, and zero slip elsewhere. The solution to the second-order linear ODE above is the sum of a particular solution satisfying the ODE (here, a uniform slip profile) and the general solution to the homogeneous version of the ODE:

$$\mathcal{D}(y) = \frac{\Delta\tau}{\bar{\mathcal{K}}_L} + Ae^{\kappa y} + Be^{-\kappa y} \tag{25}$$

where $\kappa = \sqrt{\bar{\mathcal{K}}_L / \bar{\mathcal{K}}}$. The constants A and B are determined by enforcing the boundary conditions at the rupture tips, $\mathcal{D}(\pm r/2) = 0$:

$$A = B = -\frac{\Delta\tau}{2\bar{\mathcal{K}}_L \cosh(\kappa r/2)} \tag{26}$$

Thus, the slip profile is

$$\mathcal{D}(y) = \frac{\Delta\tau}{\bar{\mathcal{K}}_L} \left(1 - \frac{\cosh(\kappa y)}{\cosh(\kappa r/2)} \right) \tag{27}$$

Figure S7 shows the resulting slip profiles for a range of values of the dimensionless number κr. For large κr values, the slip is flat over most of the rupture, as in pulse-like ruptures, with slip approximately equal to $\Delta\tau/\bar{\mathcal{K}}_L$.

Comparison between LVFZ and BK kernels. For a LVFZ model, we rewrite the kernel given in Eq. (17) as:

$$\mathcal{K}(k) = \frac{1}{2}\mu_d |k| \left(\frac{1 + (1-\Delta)\tanh(1-\Delta)}{1 - \Delta + \tanh(h|k|)} \right) \tag{28}$$

In a highly damaged fault zone where $\Delta \to 1$, the kernel reduces to:

$$\mathcal{K}(k) \approx \frac{1}{2}\mu_d|k| \left(\frac{1}{1-\Delta+\tanh(h|k|)} \right) \tag{29}$$

The high-frequency regime is defined by $\tanh(h|k|) \gg 1-\Delta$ and leads to:

$$\mathcal{K}(k) \approx \frac{1}{2}\mu_d|k| \coth(h|k|) \tag{30}$$

Moreover, if $h|k| \ll 1$, by Taylor expansion we obtain:

$$\mathcal{K}(k) \approx \frac{\mu_d}{2h} + \frac{1}{6}\mu_d h k^2 \tag{31}$$

This shows that, under certain conditions for $h|k|$, the stress transfer of the LVFZ model is equivalent to that of the BK model, with the following formal analogies:

$$\bar{\mathcal{K}}_L = \frac{\mu_d}{2h} \tag{32}$$

$$\bar{\mathcal{K}} = \frac{\mu_d h}{6} \tag{33}$$

Figure S8a shows the LVFZ kernels (Eq. 17) for various damage levels and their BK-like approximation (Eq. 31). Figure S8 shows their ratio as a function of normalized wavenumber kh and for all damage levels Δ above 0.5. The bandwidth over which the two kernels agree expands with increasing damage.

Under the conditions described above, the similarity between the LVFZ and BK kernels implies a formal analogy between the two models, which we now exploit to develop implications on pulse-like rupture. Eqs. (32) and (33) give $\kappa = \sqrt{3}/h$. The condition $\kappa r \gg 1$ for a flat, pulse-like slip profile in the BK model becomes, for the LVFZ model, $r \gg h/\sqrt{3}$. Under that condition and assuming a uniform stress drop $\Delta\tau$, a LVFZ produces ruptures

with the flat slip profile characteristic of pulses and average slip of

$$\mathcal{D} \approx \frac{\Delta\tau}{\bar{\mathcal{K}}_L} = \frac{2h\Delta\tau}{(1-\Delta)\mu} \tag{34}$$

In the low-frequency regime defined by $\tanh(h|k|) \ll 1-\Delta$, the LVFZ is too narrow to have an effect on the stress transfer, and the kernel tends to that of a homogeneous medium:

$$\mathcal{K}(k) \approx \frac{1}{2}\mu|k| \tag{35}$$

References

Ampuero, J.-P., Vilotte, J.-P., & Sanchez-Sesma, F. (2002). Nucleation of rupture under slip dependent friction law: simple models of fault zone. *Journal of Geophysical Research: Solid Earth*, *107*(B12).

Ben-Zion, Y., Peng, Z., Okaya, D., Seeber, L., Armbruster, J. G., Ozer, N., ... Aktar, M. (2003). A shallow fault-zone structure illuminated by trapped waves in the Karadere–Duzce branch of the North Anatolian Fault, western Turkey. *Geophysical Journal International*, *152*(3), 699–717.

Burridge, R., & Knopoff, L. (1967). Model and theoretical seismicity. *Bulletin of the seismological society of america*, *57*(3), 341–371.

Cochard, A., & Rice, J. R. (1997). A spectral method for numerical elastodynamic fracture analysis without spatial replication of the rupture event. *Journal of the Mechanics and Physics of Solids*, *45*(8), 1393–1418.

Cochran, E. S., Li, Y.-G., Shearer, P. M., Barbot, S., Fialko, Y., & Vidale, J. E. (2009). Seismic and geodetic evidence for extensive, long-lived fault damage zones. *Geology*,

37(4), 315–318.

Dieterich, J. H. (1981). Constitutive properties of faults with simulated gouge. *Mechanical behavior of crustal rocks: the Handin volume*, *24*, 103–120.

Huang, Y., Ampuero, J.-P., & Helmberger, D. V. (2014). Earthquake ruptures modulated by waves in damaged fault zones. *Journal of Geophysical Research: Solid Earth*, *119*(4), 3133–3154.

Kaneko, Y., Ampuero, J.-P., & Lapusta, N. (2011). Spectral-element simulations of long-term fault slip: Effect of low-rigidity layers on earthquake-cycle dynamics. *Journal of Geophysical Research: Solid Earth*, *116*(B10).

Lewis, M., Peng, Z., Ben-Zion, Y., & Vernon, F. (2005). Shallow seismic trapping structure in the san jacinto fault zone near anza, california. *Geophysical Journal International*, *162*(3), 867–881.

Lewis, M. A., & Ben-Zion, Y. (2010). Diversity of fault zone damage and trapping structures in the Parkfield section of the San Andreas Fault from comprehensive analysis of near fault seismograms. *Geophysical Journal International*, *183*(3), 1579–1595.

Li, H., Zhu, L., & Yang, H. (2007). High-resolution structures of the Landers fault zone inferred from aftershock waveform data. *Geophysical Journal International*, *171*(3), 1295–1307.

Li, Y.-G., Chen, P., Cochran, E. S., Vidale, J. E., & Burdette, T. (2006). Seismic evidence for rock damage and healing on the san andreas fault associated with the 2004 m 6.0 parkfield earthquake. *Bulletin of the Seismological Society of America*,

96(4B), S349–S363.

Li, Y.-G., Vidale, J. E., Day, S. M., & Oglesby, D. D. (2002). Study of the 1999 M 7.1 Hector Mine, California, earthquake fault plane by trapped waves. *Bulletin of the Seismological Society of America*, *92*(4), 1318–1332.

Luo, Y., Ampuero, J.-P., Galvez, P., van den Ende, M., & Idini, B. (2017). *QDYN: a Quasi-DYNamic earthquake simulator (v1.1).* Zenodo. (doi:10.5281/zenodo.322459)

Mizuno, T., Kuwahara, Y., Ito, H., & Nishigami, K. (2008). Spatial variations in fault-zone structure along the nojima fault, central japan, as inferred from borehole observations of fault-zone trapped waves. *Bulletin of the Seismological Society of America*, *98*(2), 558–570.

Peng, Z., Ben-Zion, Y., Michael, A. J., & Zhu, L. (2003). Quantitative analysis of seismic fault zone waves in the rupture zone of the 1992 landers, california, earthquake: evidence for a shallow trapping structure. *Geophysical Journal International*, *155*(3), 1021–1041.

Rice, J. R. (1993). Spatio-temporal complexity of slip on a fault. *Journal of Geophysical Research: Solid Earth*, *98*(B6), 9885–9907.

Rubin, A., & Ampuero, J.-P. (2005). Earthquake nucleation on (aging) rate and state faults. *J. Geophys. Res.-Sol. Ea.*, *110*(B11).

Ruina, A. (1980). Friction laws and instabilities: a quasi-static analysis of some dry friction behaviour. *Ph. D. thesis, Division of Engineering, Brown University*.

Ruina, A. (1983). Slip instability and state variable friction laws. *J. Geophys. Res.-Sol. Ea.*, *88*(B12), 10359–10370.

Yang, H., & Zhu, L. (2010). Shallow low-velocity zone of the San Jacinto fault from local earthquake waveform modelling. *Geophysical Journal International*, *183*(1), 421–432.

Yang, H., Zhu, L., & Cochran, E. S. (2011). Seismic structures of the calico fault zone inferred from local earthquake travel time modelling. *Geophysical Journal International*, *186*(2), 760–770.

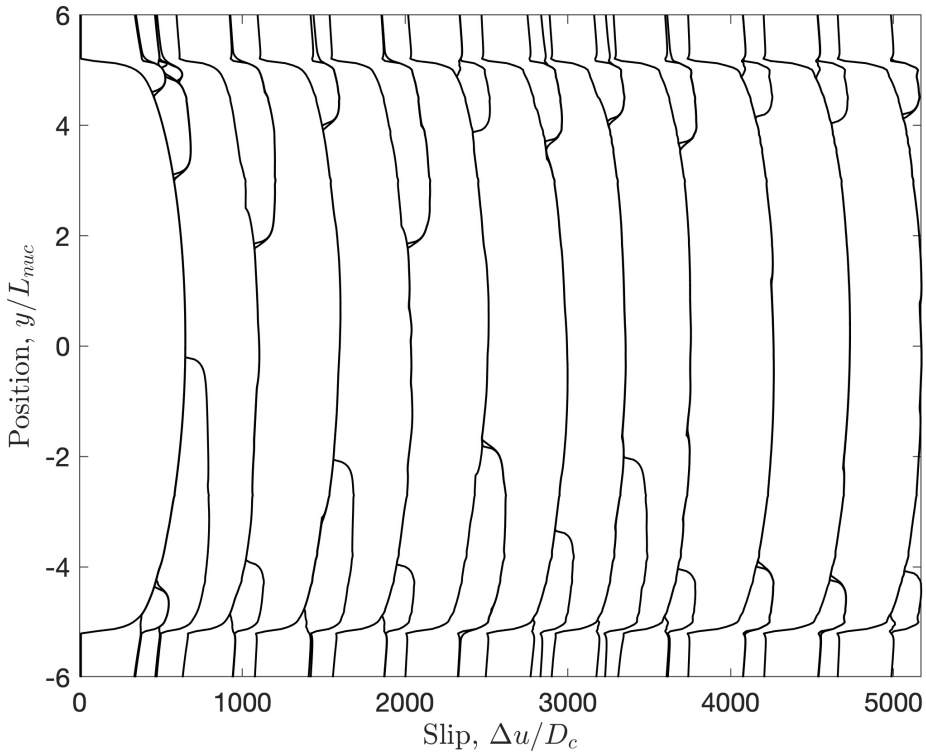

Figure S1. History of seismic activity in a simulation of a fault model with $\Delta = 0.9$ and $2h \approx 1/40 L_{vw}$. Solid lines represent accumulated slip after an earthquake occurs.

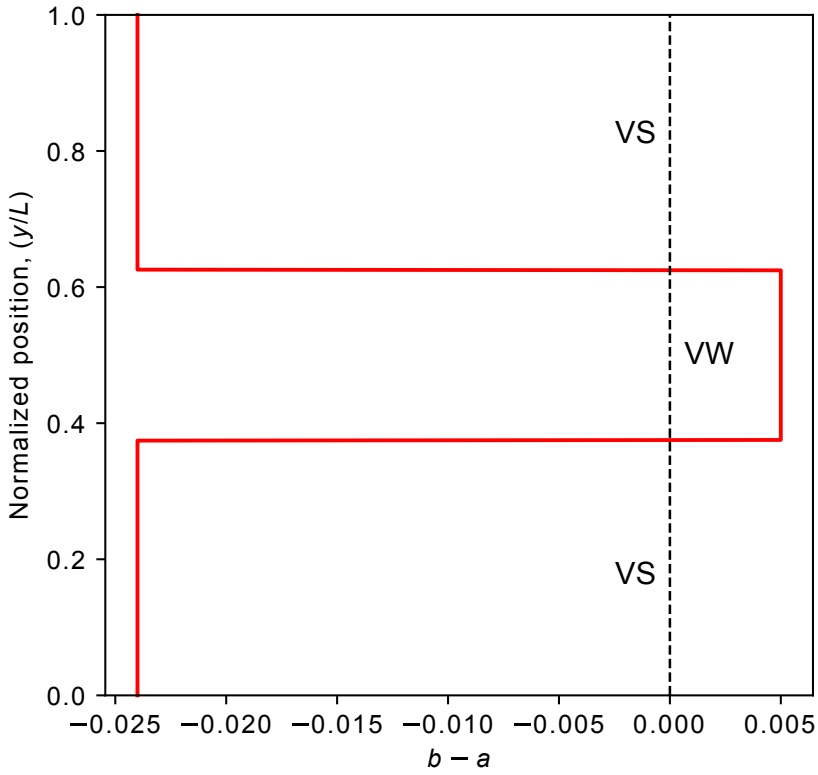

Figure S2. The $b-a$ parameter along position in the fault. The seismogenic zone is indicated as a velocity-weakening zone (VW) surrounded by two stably sliding velocity-strengthening (VS) segments.

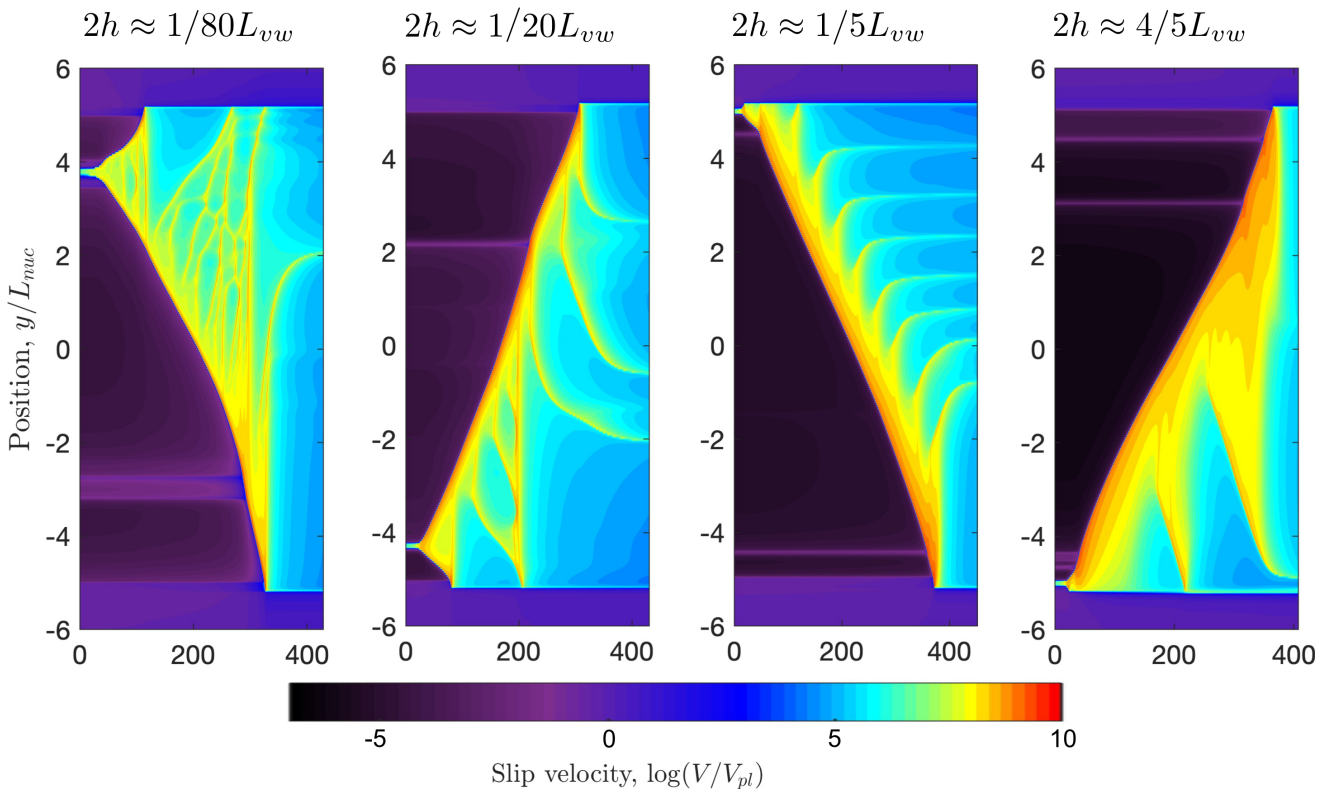

Figure S3. Spatiotemporal evolution of slip rate in the characteristic event of earthquake cycle models using a LVFZ with $\Delta = 0.9$ and different values of damage zone thickness.

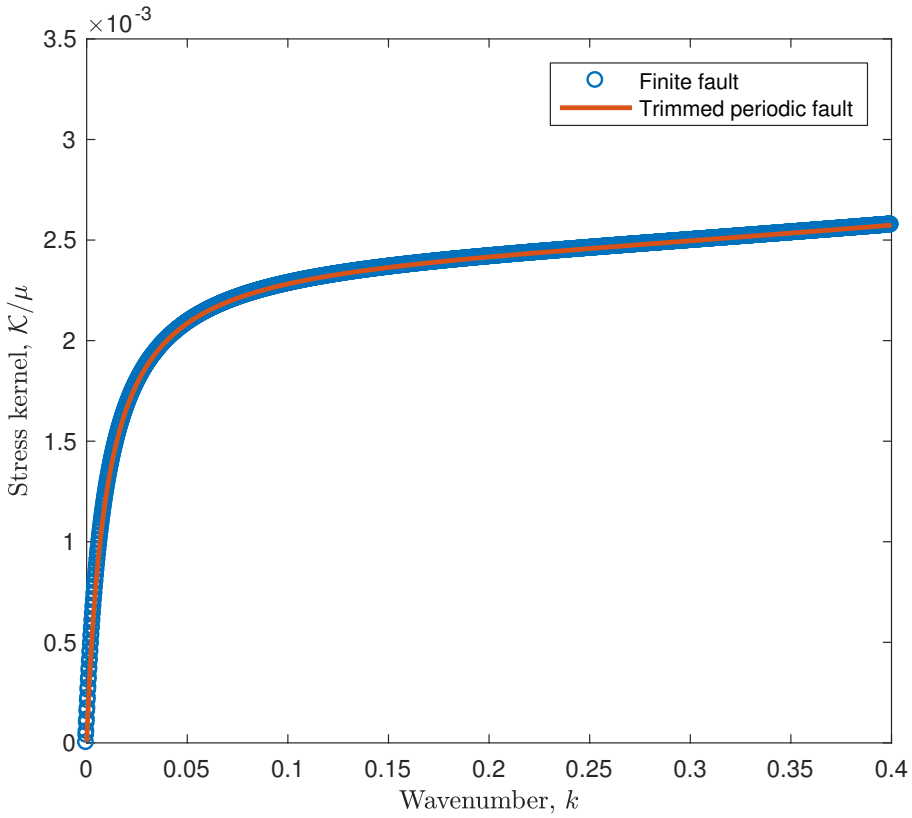

Figure S4. Static stress kernel in a LVFZ versus wavenumber based on two numerical implementations. The blue circles represent the combination of the kernel of a finite fault with Eq. (17) in the wavenumber domain. The continuous orange line is an approximated kernel using Eq. (17) over a periodic fault 32 times longer.

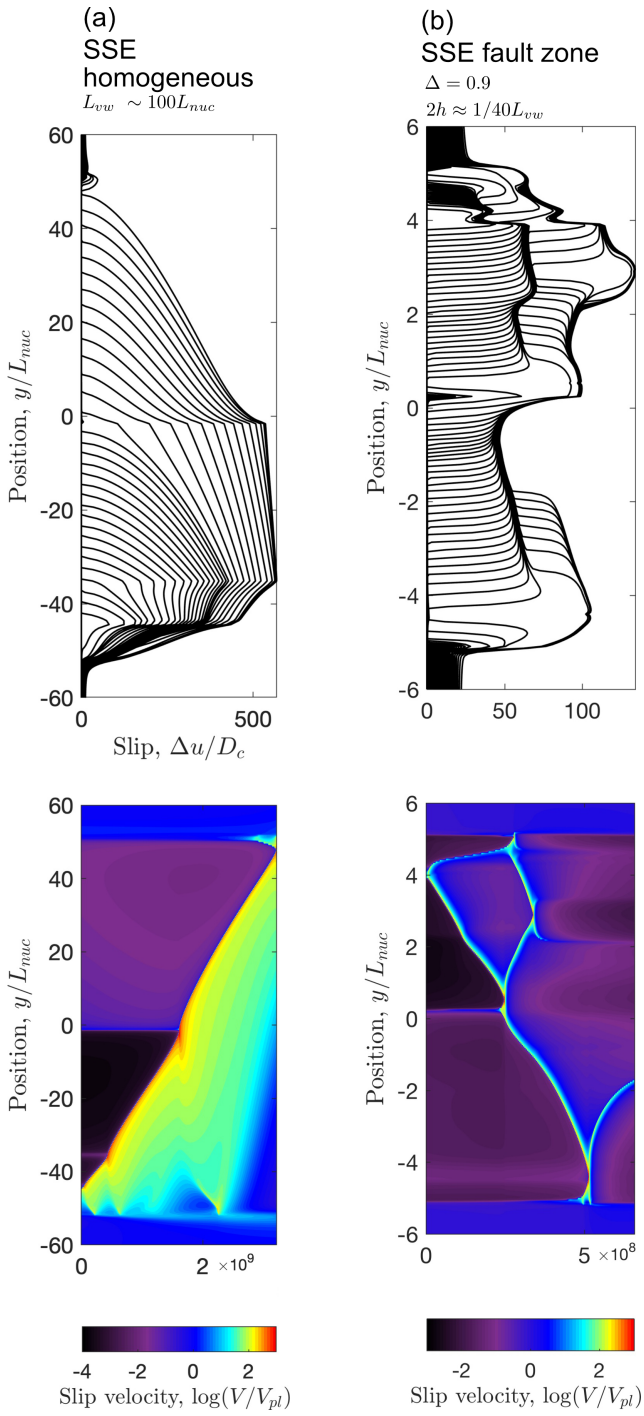

Figure S5. Comparison of slow-slip earthquakes (SSE) with and without a fault zone (LVFZ) modeled using a friction law of increased velocity-strengthening. (a) A slow earthquake in a fully-damaged homogeneous medium. The slip profiles are indicative of crack-like rupture propagation. (b) The addition of the LVFZ promotes multiple back-propagating secondary fronts. The main and secondary fronts show slip profiles indicative of pulse-like rupture propagation.

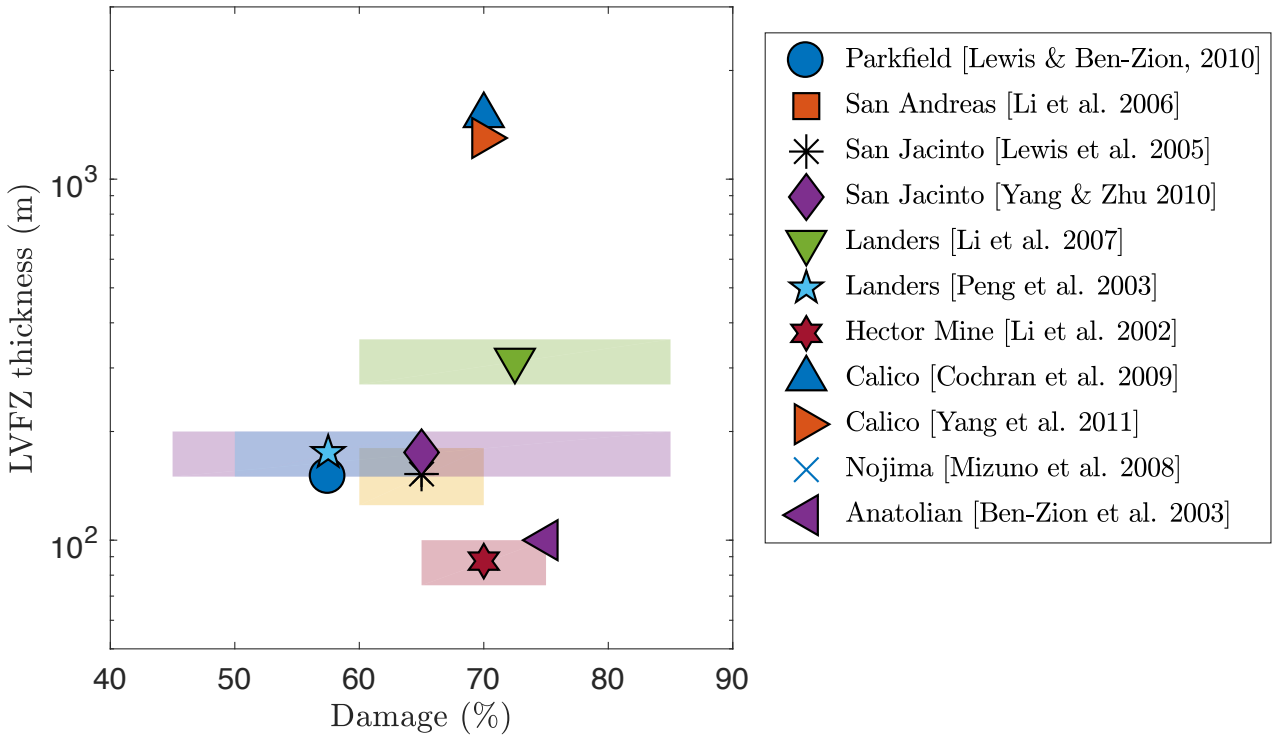

Figure S6. A compilation of fault-zone properties included in Huang et al. (2014). Damage represents a reduction in shear moduli, which relates to a reduction in velocity as $\Delta_\mu = 1-(1-\Delta_v)^2$, were Δ_μ is the damage reported in the figure and Δ_v the reduction in velocity reported in Huang et al. (2014).

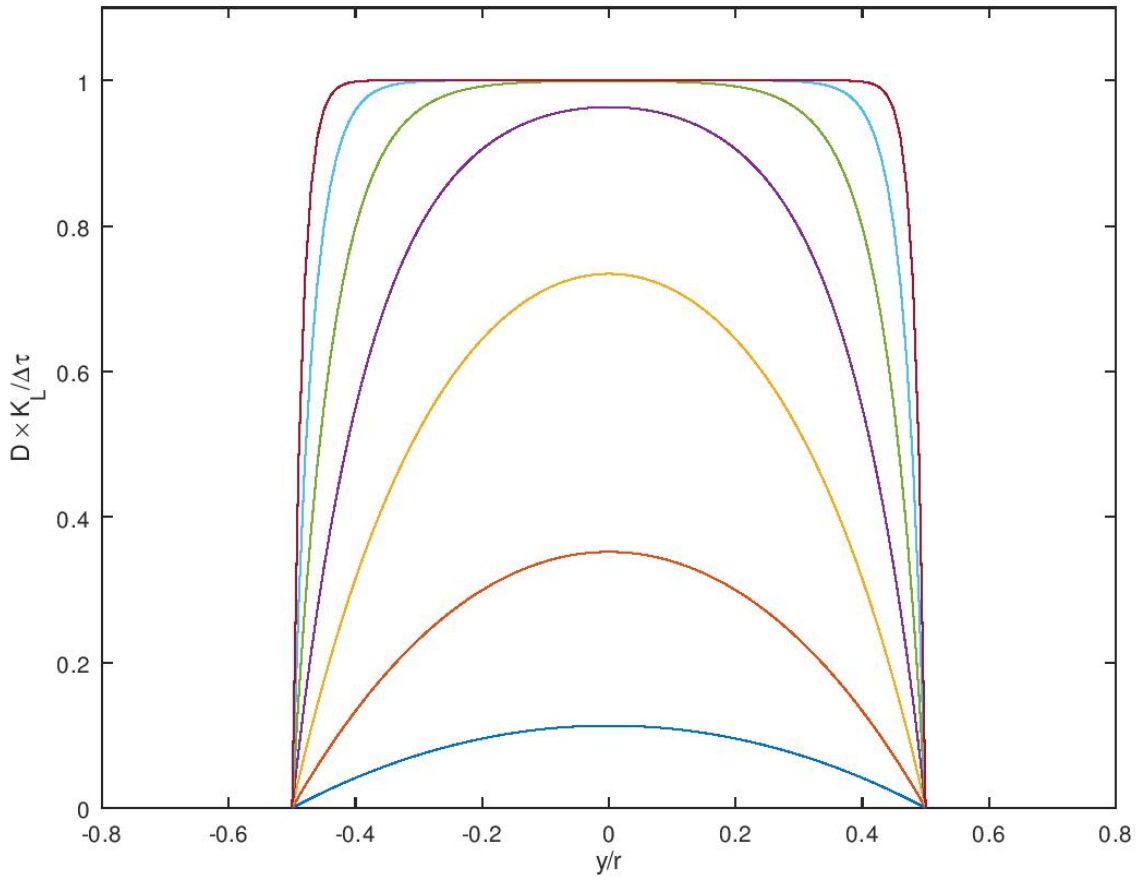

Figure S7. Static slip profiles for ruptures with uniform stress drop $\Delta\tau$ in a continuum Burridge-Knopoff model, with loading stiffness K_L. Each curve is for a different value of κr in $\{1, 2, 4, 8, 16, 32, 64\}$, from bottom to top.

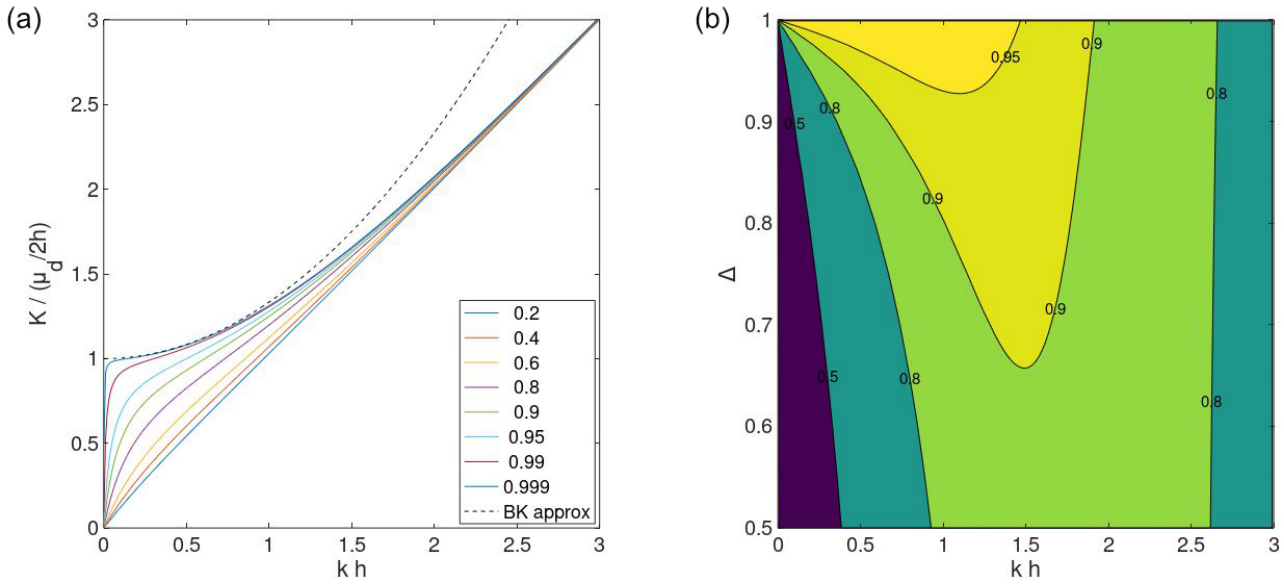

Figure S8. Comparison of LVFZ and BK static stress transfer kernels. (a) LVFZ kernels for a range of damage levels Δ (see legend) and their BK approximation (dashed) as a function of normalized wavenumber kh. Kernels are normalized by $\mu_d/2h$. (b) Ratio between LVFZ kernels and their BK-like approximation, as a function of kh and damage level Δ. The bandwidth over which the two kernels agree expands with increasing damage (see for instance the contours 0.9 and 0.95).

Table S1. Approximated dimensions of a fault and properties of the rupture in the homogeneous and LVFZ models shown in Fig. 3 after assuming a value for D_c.

	Homogeneous	LVFZ ($\Delta = 0.9$)
Characteristic slip, D_c	2 mm	2 mm
Seismogenic zone, L_{vw}	2.5 km	2.5 km
Nucleation length, L_{nuc} and L^*_{nuc}	242 m	40 m
Fault-zone thickness, $2h$	-	64 m
Event duration, t	2.4 sec	32.4 sec
Average rise-time	2.1 sec	5.6 sec

Table S2. Parameters used in the numerical simulations.

Parameter	Symbol	Value
Direct effect (VW/VS)	a	0.014/0.043
Evolution effect (VW/VS)	b	0.019/0.019
Characteristic slip	D_c	2 mm
Tectonic loading	V_{pl}	10^{-9} m/s
Reference slip rate	V_0	10^{-9} m/s
Reference friction coefficient	μ_0	0.6
Shear-wave speed	β	3.5 km/s
Intact shear modulus	μ	30 GPa
Effective normal stress	σ	120 MPa